Research Square

Preprints are preliminary reports that have not undergone peer review.
They should not be considered conclusive, used to inform clinical practice,
or referenced by the media as validated information.

Intelligence-Driven Three-Dimensional Route Loading for Resource-Efficient Freight Operations

Junling Zhu
Zhaoqing University
Tang-Xi Chen
Fujian Polytechnic Normal University
Yujie Lin
Zhaoqing University
Shiyi Tan
s1080348710@m108.nthu.edu.tw

Zhaoqing University
Mingjun Qiu
Zhaoqing University

Research Article

Keywords: computational intelligence, three-dimensional loading, vehicle routing, adaptive large-neighborhood search, fleet consolidation, resource efficiency, sustainable freight

Posted Date: November 11th, 2026

DOI: https://doi.org/10.21203/rs.3.rs-11211602/v1

License: This work is licensed under a Creative Commons Attribution 4.0 International License.
Read Full License

Additional Declarations: No competing interests reported.

Research

Intelligence-Driven Three-Dimensional Route Loading for Resource-Efficient Freight Operations

Junling Zhu[1], Tang-Xi Chen[2], Yujie Lin[1],Shiyi Tan[1]* and Mingjun Qiu[1]

Corresponding authors: Shiyi Tan

E-mail addresses: s108034871@m108.nthu.edu.tw

[1] School of Computer Science and Software, Zhaoqing University, Zhaoqing 526061, China

[2] Ocean College, Fujian Polytechnic Normal University, Fuqing 350300, Fujian, China

Abstract

Digital freight systems become resource-efficient when order, routing and loading data are converted into executable decisions. This study formulates customer-indivisible three-dimensional route loading for homogeneous vehicles as a lexicographic optimization problem that minimizes certified fleet size before route distance. An intelligence-driven hierarchical adaptive large-neighborhood search (H-ALNS) couples dual certified initialization, geographic reassignment, whole-vehicle closure, two-route exchange, three-route ejection, failure-class feedback and adaptive depth-first packing. Every accepted route is reconstructed at coordinate level and checked by a common validator. Sustainability is measured through vehicles required for fixed order demand and fleet intensity per customer and item, linking computational intelligence to resource efficiency rather than treating geometric fill as a proxy. Evaluation covers 600 benchmark instances spanning 20, 60 and 100 customers, 200 and 400 items, and 3, 10 and 100 box types. H-ALNS reduces the aggregate fleet from 9346 to 7915 vehicles, avoiding 1431 dispatches (15.31%). Vehicle demand falls in 340 instances and remains equal in 260, with no increase; positive aggregate reductions occur in all 18 strata and reach 22.30%. Fleet intensity decreases from 22.91 to 19.40 vehicles per 100 customers and from 51.92 to 43.97 vehicles per 1000 items. The results show that adaptive route restructuring produces resource gains when customer regrouping is certified as complete three-dimensional layouts. The resulting decision object—routes, item coordinates, a feasibility certificate and fleet-resource measures—supports resource-efficient freight planning in intelligent logistics systems.

Keywords: computational intelligence; three-dimensional loading; vehicle routing; adaptive large-neighborhood search; fleet consolidation; resource efficiency; sustainable freight

1. Introduction

Industry 4.0 has transformed logistics from a sequence of isolated activities into a digitally coordinated decision system. Barreto et al. showed how warehouse management, transport management and intelligent transport technologies connect logistics information across operational stages [1]. Yavas and Ozkan-Ozen extended this architecture to logistics centers, where digital technologies reshape warehousing, handling

and transport activities [2]. Winkelhaus and Grosse identified sustainability as a defining dimension of Logistics 4.0 [3]. The common implication is that logistics intelligence should convert data into operational decisions whose resource consequences can be measured.

For freight operations, resource efficiency is expressed through the transport capacity deployed to serve a given order demand. This principle is consistent with the resource-efficiency orientation of Sustainable Development Goal 8 [4] and the responsible-production orientation of Sustainable Development Goal 12 [5]. A decision is therefore more than computationally successful when it reduces the fleet resources required for the same customer and item demand while retaining an executable transport plan.

Three-dimensional loading is the physical decision layer at which that objective becomes concrete. George and Robinson established rectangular-box placement as a computational optimization problem [6]. Bischoff and Ratcliff subsequently showed that useful loading methods must represent operational requirements in addition to geometric compactness [7]. In multi-customer freight, the outer decision assigns and sequences customers, while the inner decision assigns coordinates to every item. A customer combination can reduce fleet demand only when all affected routes satisfy capacity and time windows and every affected vehicle admits a complete 3D layout.

This coupling changes the role of computational intelligence. The search process must learn which route transformations create packable customer groups, reconstruct affected loads, certify the result and return the outcome as feedback to the next decision. Fleet consolidation is consequently an integer threshold reached by a closed route–packing loop, not a smooth consequence of higher volume utilization. Route distance remains a secondary operational measure that distinguishes alternatives within the same certified fleet layer.

This study develops a hierarchical adaptive large-neighborhood search (H-ALNS) for customer-indivisible three-dimensional route loading. The method integrates dual certified initialization, geographic customer reassignment, whole-vehicle closure, two-route exchange, three-route ejection, failure-class operator learning and adaptive depth-first coordinate reconstruction. Its contribution is a decision architecture in which customer-level proposals, item-level layouts, feasibility certification and fleet-resource measures are parts of one auditable object. The complete evaluation covers 600 benchmark instances and all 18 combinations of customer count, item count and box-type heterogeneity.

2. Literature foundation and research positioning

2.1. From Geometric Construction to Practical Loading

Research on three-dimensional loading first concentrated on constructing dense layouts from a continuous coordinate space. Crainic et al. generated extreme points from the boundaries of placed items, thereby reducing coordinate search to a finite set of geometrically meaningful candidates [8]. Gehring and Bortfeldt used a genetic algorithm to optimize item sequences before deterministic placement [9]. Gonçalves and

Resende separated global search from packing evaluation through a biased random-key representation [10]. These approaches established a common architecture in which the outer algorithm proposes an order and the decoder determines whether that order becomes a complete layout.

Practical feasibility added a second layer to this architecture. Junqueira et al. incorporated stability and load-bearing conditions into mathematical container-loading models [11]. Davies and Bischoff showed that layouts with comparable space utilization can produce materially different weight distributions [12]. Krebs and Ehmke linked item coordinates to vehicle axle loads and demonstrated the transport relevance of longitudinal mass distribution [13]. Pollaris et al. organized loading constraints from the perspective of vehicle-routing applications and highlighted the importance of unloadability [14]. Taken together, these studies show that geometry, load transfer and delivery operations must be evaluated as parts of one loading certificate.

2.2 Resource-efficient freight and intelligent decision systems

Resource-efficient freight uses the minimum practical transport capacity for a fixed service demand. Vehicle count measures the discrete fleet resources activated by a plan, while route distance distinguishes the transport activity generated by alternative customer groups. Their joint evaluation supports the resource-efficiency principles associated with SDG 8 [4] and the responsible-production logic of SDG 12 [5]. In an intelligent decision system, these outcomes must remain linked to routes, item coordinates and feasibility evidence so that digital optimization corresponds to an executable physical plan.

2.3. Packing Search and Decoder Design

A strong route-loading method depends on the amount of useful structural information produced by its packing evaluator. Pisinger designed container-loading heuristics that exploit problem-specific ordering and placement rules [15]. Eley improved construction through block arrangements that combine items before placement [16]. Fanslau and Bortfeldt used tree search to retain alternative partial layouts and delay premature geometric commitment [17]. These methods show why a packing decoder is an active search component rather than a passive feasibility check.

Subsequent work strengthened the coupling between global sequences and local placement. Bortfeldt and Gehring combined genetic search with specialized loading construction [18]. Araya and Riff used beam search to preserve several promising partial packings [19]. Paquay et al. separated multiple-bin construction into coordinated phases [20]. Ma et al. embedded logistics information in a dedicated three-dimensional loading algorithm [21]. The shared lesson is that retaining controlled diversity inside the decoder can expose complete layouts that a single greedy path misses.

Reviews and constraint-focused models clarify which features distinguish operational loading from pure geometry. Bortfeldt and Wäscher classified the practical constraints appearing across container-loading applications [22]. Gzara et al. incorporated practical three-dimensional constraints into pallet-loading optimization [23]. Do Nasci-

mento et al. provided a comprehensive treatment of practical container-loading conditions [24]. Erbayrak et al. combined load balance and product-family considerations in a multi-objective formulation [25]. This literature supports the use of a shared certificate in which space, shipment integrity and transport-relevant conditions are evaluated together.

2.4. Integrated Routing and Three-Dimensional Loading

The integrated route-loading problem adds customer assignment and visit sequence to the packing decision. Krebs et al. assembled advanced support, bearing, reachability, axle and balance constraints within a 3L-VRPTW framework [26]. Gendreau et al. introduced the three-dimensional loading capacitated vehicle-routing problem and coupled routing search with loading heuristics [27]. Iori et al. demonstrated how exact routing methods can incorporate two-dimensional loading feasibility [28]. Fuellerer et al. used ant colony optimization with routing- and packing-specific information for the three-dimensional variant [29]. These contributions established the central decomposition used by later research: route construction supplies candidate customer groups, and a packing module certifies each route.

Local and adaptive search methods then improved the exchange of information between the two layers. Ceschia et al. developed local-search techniques tailored to a joint routing-packing problem [30]. Krebs and Ehmke released a validator and visualizer that standardize route and coordinate verification [31]. Ropke and Pisinger introduced adaptive large-neighborhood search for pickup-and-delivery routing with time windows [32]. Pisinger and Ropke generalized the framework across several vehicle-routing variants [33]. The adaptive principle is especially relevant to 3L-CVRP because neighborhoods differ markedly in geometric difficulty and evaluation cost.

2.5. Recent Route–Packing Algorithms

Recent studies have moved from generic routing neighborhoods toward more explicit coordination with the loading evaluator. Krebs et al. compared DBLF representations inside an outer ALNS and showed that the organization of free space materially affects solution quality and runtime [34]. Küçük and Yildiz formulated constraint-programming and decomposition approaches for 3L-CVRP, providing a complementary exact-modeling perspective [35]. Cen et al. combined ALNS with a multi-order packing search for a cross-docking variant [36]. Together, these studies demonstrate that outer-search performance depends on the structure and throughput of the inner packing process.

Newer formulations also broaden the operational decisions represented by the loading plan. Chi and He developed a branch-and-price framework for pickup routing with three-dimensional loading constraints [37]. Chi et al. added relocation decisions so that loading efficiency and operational handling cost can be optimized jointly [38]. Zhang et al. introduced a knowledge-guided insertion operator that adapts neighborhood scale to the routing-packing structure [39]. These contributions support structural customer moves and bounded ejection mechanisms as a principled alternative to repeated single-customer insertion.

2.6 Adaptive search and integrated freight operations

Problem-specific adaptation has also proved valuable beyond the basic 3L-CVRP. Voigt et al. combined ALNS with population-based recombination for routing problems that include depot-location decisions [40]. Friedrich and Elbert embedded neighborhood search and route recombination in a city-logistics problem with transshipment facilities [41]. These algorithms show that adaptive search becomes most effective when operator rewards correspond to the actual structural objective.

Unloading research provides a direct operational counterpart to vehicle consolidation. Bonet Filella et al. modeled unloading interference as a relocation penalty and improved solutions by destroying and reconstructing high-penalty packing regions [42]. Nascimento et al. used logic-based Benders decomposition to connect routing decisions with exact and heuristic packing-feasibility checks [43]. Yıldız et al. integrated customer orders, three-dimensional loading and routing in an industrial cable-distribution case [44]. This line of work confirms that packing, customer grouping and transport execution should be represented within the same decision system.

The search literature supplies further evidence for combining exact structure with scalable neighborhoods. Rajaei et al. addressed large-scale split-delivery routing with heterogeneous vehicles and three-dimensional loading [45]. Ruan et al. developed a hybrid algorithm that coordinates routing search with an improved packing procedure [46]. Efron and Tibshirani established bootstrap resampling as a distribution-free method for quantifying empirical uncertainty [47]. The Krebs benchmark repository provides the 600-instance factorial design used in the present experiment [48]. Collectively, these sources motivate an evaluation that reports certified fleet effects, their variation across instance strata and the route-distance consequences of customer consolidation.

3. Problem Formulation

3.1. Sets, Decisions and Feasibility Certificate

Let C be the customer set, I the item set and V the available homogeneous vehicle slots. Item i has customer c(i), dimensions (l_i,w_i,h_i), mass m_i and an admissible upright orientation. A solution assigns every customer and all associated items to one active vehicle, determines a route for each vehicle and produces item coordinates. The feasibility certificate combines customer coverage, payload capacity, time-window feasibility, three-dimensional containment and pairwise non-overlap.

$$\sum_{v\in V} a_{iv} = 1, \quad a_{iv} \le y_v, \quad \forall i \in I \tag{1}$$

$$a_{iv} = a_{jv}, \quad \forall i,j \in I: c(i) = c(j), \forall v \in V \tag{2}$$

$$\sum_{i\in I} m_i\, a_{iv} \le Q y_v, \quad \forall v \in V \tag{3}$$

Table 1 Principal notation

Symbol	Definition	Role
I, C, V	Items, customers and candidate vehicle slots	Input
a_iv, y_v	Item assignment and vehicle activation	Decision

Symbol	Definition	Role
π_v	Customer route of vehicle v	Decision
x_i, y_i, z_i	Lower-front-left item coordinates	Decision
N	Number of active certified vehicles	Primary objective
D	Total route distance	Secondary objective
ΔN, ΔD	Avoided vehicles and route-distance change	Outcome

Table 1 separates the instance sets and route-loading decisions from the fleet and distance quantities used in the objective and evaluation layers. This notation keeps customer assignment, item coordinates and certified resource outcomes distinct throughout the formulation.

3.2. Geometric Feasibility

$$0 \le x_i, 0 \le y_i, 0 \le z_i, \;\; x_i + l_i^o \le L, y_i + w_i^o \le W, z_i + h_i \le H \tag{4}$$

For any pair assigned to the same vehicle, at least one separating relation holds along the longitudinal, lateral or vertical axis. Upright rotation exchanges item length and width while retaining height. The common validator receives the complete customer routes and item coordinates and returns the benchmark feasibility decision.

3.3. Lexicographic Fleet–Distance Objective

$$\min lex\, f(x) = \big(N(x), D(x)\big) \tag{5}$$

$$N(x) = \sum_{v \in V} y_v, D(x) = \sum_{v \in V: y_v = 1} \sum_{(p,q) \in A(\pi_v))} d_{pq} \tag{6}$$

Equation (5) assigns strict priority to the number of certified vehicles. Route distance distinguishes solutions only within the same fleet layer. This hierarchy matches the operational mechanism of vehicle closure: a decrease in N changes the number of dispatches, while D records the routing consequence of the new customer combination.

3.4. Fleet and Route-Efficiency Measures

$$\Delta N = N(x_0) - N(x_1) \tag{7}$$

$$\Delta D = D(x_1) - D(x_0) \tag{8}$$

$$\rho_N = \frac{\Delta N}{N(x_0)} \times 100\% \tag{9}$$

$$FRI_{C(x)} = \frac{100N(x)}{|C|}, FRI_{I(x)} = \frac{1000N(x)}{|I|} \tag{10}$$

Equation (7) measures avoided vehicle dispatches, Equation (8) records the route-distance consequence of customer regrouping and Equation (9) normalizes fleet consolidation against the initial plan. Equation (10) reports fleet-resource intensity as vehicles per 100 customers and per 1000 items. Together, these measures distinguish structural vehicle closure from same-fleet route refinement and relate fleet demand to a fixed service volume.

4. Intelligence-driven hierarchical adaptive large-neighborhood search

H-ALNS operates as a closed intelligence loop between customer grouping and physical reconstruction. Its hierarchy first searches for a certified reduction in active vehicles and then uses route distance to distinguish alternatives within the same fleet layer. Successful certified layouts reinforce the responsible neighborhood, while classified failures redirect operator selection toward the capacity, scheduling or geometric barrier encountered during reconstruction. Fig. 1 summarizes the resulting chain from digital freight data to an auditable fleet-resource outcome.

4.1. Certified Dual Initialization

H-ALNS begins from two constructive views of the same instance. The beam-1 initializer emphasizes fast deterministic completion, whereas beam-5 retains five promising partial packing states and enlarges geometric diversity. Both initializers use the common benchmark route-loading model. The lexicographically best certified result becomes the incumbent, giving every subsequent comparison a coordinate-level reference.

4.2. Fleet-Closing Search Hierarchy

The search hierarchy concentrates computational effort on vehicle closure. Low-utilization donor routes and geographically compatible receivers receive priority. A geographic move transfers a customer toward a nearby compatible route; whole-route closure redistributes every customer of a selected donor; and route distance orders equal-fleet candidates. Fast capacity and time-window screens precede the physical decoder, so expensive geometric evaluation is reserved for structurally plausible combinations.

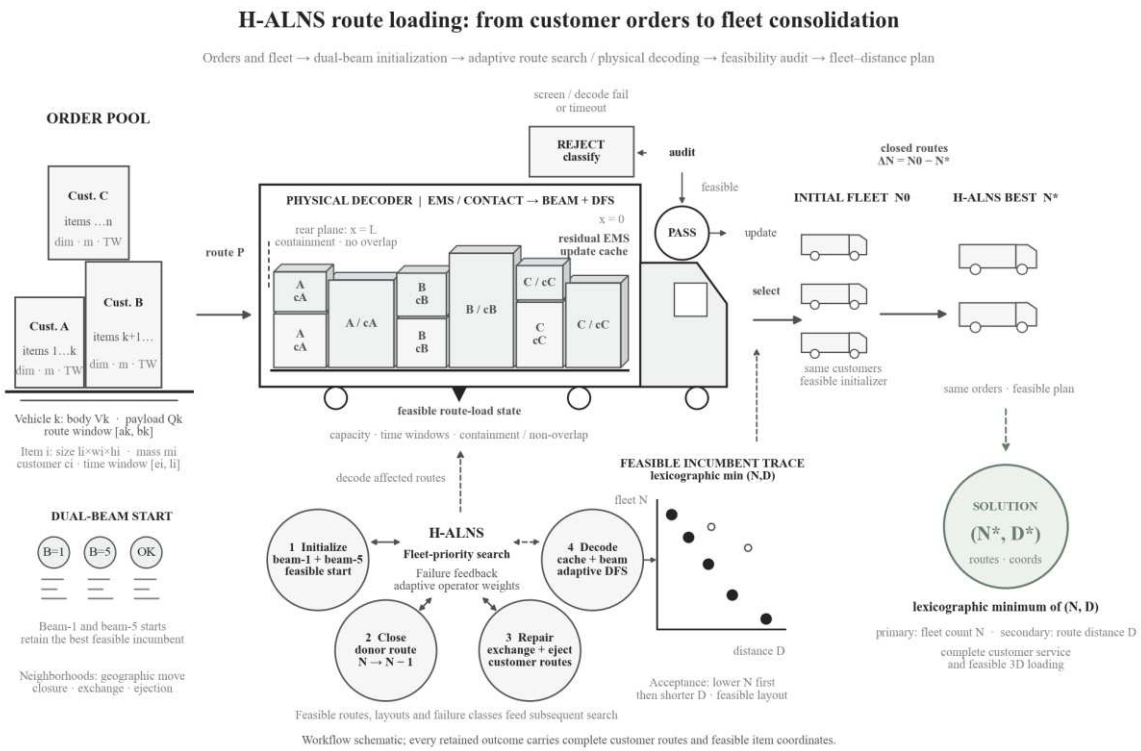


Fig. 1 Closed-loop intelligence connects digital freight data, route restructuring, 3D reconstruction, certification and fleet-resource outcomes

The workflow separates proposal generation from admissibility without separating their feedback. Fleet-closing operators determine which customer combinations are tested, while the decoder determines whether those combinations become complete coordinate solutions. Certified success rewards the responsible neighborhood; classified failure redirects subsequent operator selection toward the structural barrier encountered during reconstruction.

4.3. Two-Route Exchange and Three-Route Ejection

A direct insertion can fail because the receiving route has an unfavorable combination of residual payload, time-window position and three-dimensional shape. The two-route exchange replaces one receiver customer with a donor customer and reconstructs both loads. The three-route ejection chain extends this mechanism: a donor customer enters route r1, a displaced customer moves from r1 to r2, and the resulting three affected layouts are evaluated as one structural move. This bounded chain supplies a wider scheduling effect while preserving a tractable evaluation scope.

4.4. Adaptive DFS Physical Evaluator

For each affected route, the decoder first queries the seeded layout cache. New layouts are constructed from maximal empty spaces and contact-derived positions. Beam construction resolves the early high-branching stage, while adaptive DFS focuses on the residual items that determine completion. The search order responds to capacity saturation, route incompatibility and geometric dead ends. Only complete benchmark-certified layouts return a fleet-distance value to the outer search.

Fig. 2 opens the common decoder at coordinate level. Customer colors remain unchanged between route reassignment and packing, making customer indivisibility visible throughout the search. The vehicle coordinate system defines the placement domain; solid cuboids denote accepted placements, the dashed volume denotes a residual maximal empty space and marked contact points define geometrically meaningful candidate anchors.

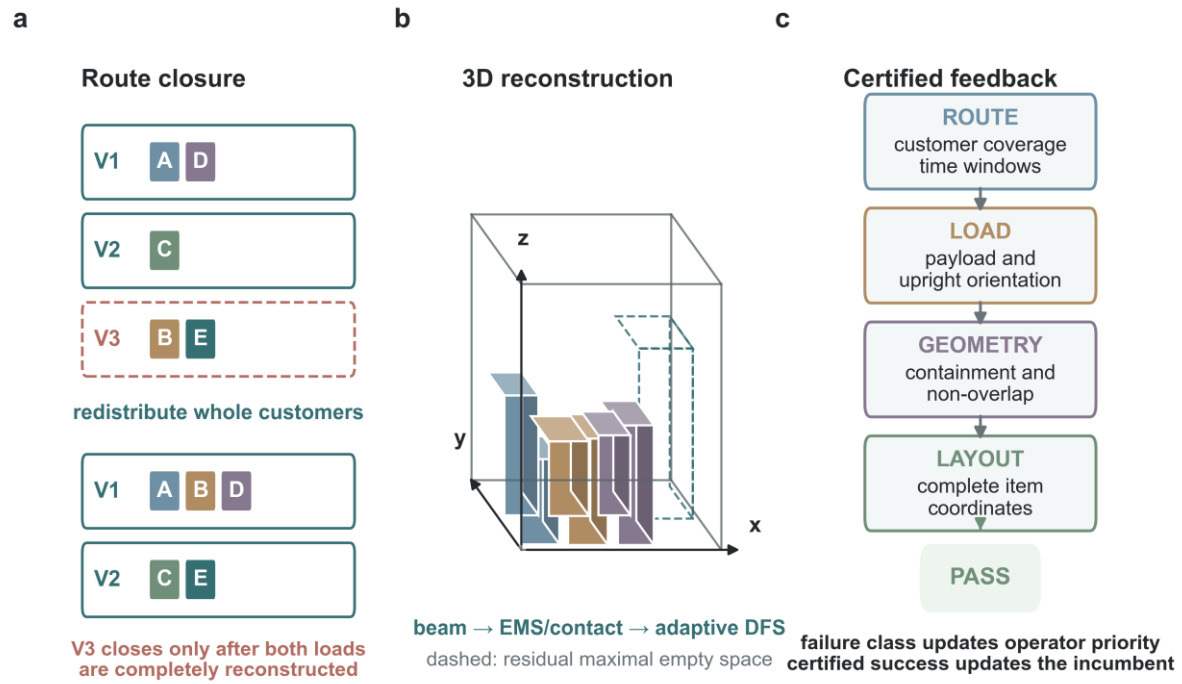


Fig. 2 Vehicle closure couples whole-customer reassignment with coordinate-level reconstruction and certified feedback

The coordinate mechanism turns physical feasibility into search information. Each accepted placement changes the residual empty-space structure, each completed route becomes a reusable cache entry and each failed reconstruction identifies whether the current barrier originates from route structure, capacity, time windows or three-dimensional geometry. The outer H-ALNS therefore learns from certified loading outcomes rather than from an abstract customer assignment alone.

4.5. Failure Feedback and Operator Learning

Each operator receives feedback from the certified outcome of its proposal. Fleet reduction receives the strongest reward, same-fleet distance improvement receives the next reward and physically complete reconstruction supplies a feasibility reward. Failure categories update the relative selection pressure of geographic reassignment, exchange, ejection and reconstruction. The resulting feedback loop aligns neighborhood choice with the current structural barrier instead of applying one placement rule uniformly throughout the run.

Algorithm 1 Intelligence-driven H-ALNS for certified fleet consolidation

Algorithm 1. Hierarchical adaptive large-neighborhood search for certified fleet consolidation

Input	**Benchmark instance Ω; wall-clock budget T; random seed s.**
PHASE I	**CERTIFIED INITIALIZATION**
	Construct S1 with beam width 1 and certify its routes and coordinates.
	Construct S5 with beam width 5 and certify its routes and coordinates.
	Set S* to the lexicographically better certified solution in {S1, S5}.
	Initialize layout cache C, operator weights w and failure statistics h.
PHASE II	**FLEET-CLOSING SEARCH**
while	elapsed time < T do
	Select an operator o from w and identify a donor route plus compatible receivers.
	Generate a geographic move, whole-route closure, two-route exchange or three-route ejection proposal P.
if	capacity, time-window or geographic screening rejects P then
	Record the structural failure in h and reweight operator o.
	continue with the next neighborhood proposal.
end if	
PHASE III	**COORDINATE RECONSTRUCTION**
for	each route r affected by P do
	Query C with the customer set, visit order and item attributes of r.
if	a certified cached layout is unavailable then
	Generate maximal-empty-space and contact-derived candidate positions.
	Apply beam construction to retain diverse partial packing states.
	Apply adaptive DFS to complete the residual items under route-loading geometry.
	Store every completed route layout and its coordinates in C.
end if	
end for	
PHASE IV	**CERTIFICATION AND LEARNING**
if	the common benchmark validator certifies all routes and coordinates of P then
	Evaluate the lexicographic pair (N(P), D(P)).
	Reward fleet closure first, distance refinement second and feasible reconstruction third.
if	(N(P), D(P)) is lexicographically better than (N(S*), D(S*)) then
	Set S* ← P and refresh the incumbent coordinate certificate.

Input	**Benchmark instance Ω; wall-clock budget T; random seed s.**
26	***end if***
27	***else***
28	Classify the failed route-loading reconstruction and update h and w.
29	***end if***
30	***end while***
Output	Officially revalidated solution S* with item coordinates, N(S*) and D(S*).

Table 2 maps each H-ALNS component to its search mechanism and operational contribution. The upper rows describe customer-level fleet restructuring, whereas the lower rows describe coordinate reconstruction, layout reuse and final certification. Read together with Algorithm 1, the table shows how route closure pressure is coupled to complete three-dimensional feasibility rather than evaluated as an isolated routing move.

Table 2 H-ALNS components

Component	Mechanism	Contribution
Dual initializer	Beam-1 and beam-5 certified construction	Diverse, auditable starting point
Geographic move	Distance-aware whole-customer reassignment	Compatible receiver discovery
Whole-route closure	Remove a donor and reallocate its customers	Direct vehicle-count pressure
Two-route exchange	Joint reconstruction of two routes	Resolve local incompatibility
Three-route ejection	Bounded displacement chain across three routes	Escape saturated receivers
vv	Failure-guided residual packing search	Complete difficult layouts
Layout cache	Reuse certified route-loading coordinates	Increase evaluation throughput
Benchmark audit	Shared route and coordinate validator	Reproducible feasibility

5. Experimental Design

5.1. Benchmark Matrix

The experiment uses the 600-instance 3L-VRPTW benchmark introduced by Krebs et al. [48]. The design crosses three customer levels (20, 60 and 100), two item levels (200 and 400) and three box-type levels (3, 10 and 100), producing 18 strata. This factorial organization separates customer-allocation pressure, geometric scale and dimensional heterogeneity. The benchmark constraint set activates customer coverage, vehicle capacity, time windows, three-dimensional containment and non-overlap.

5.2. Execution and Evidence Protocol

All runs use the same seed and one CPU thread. Beam-1 and beam-5 construction generate the certified initializer, after which geographic reassignment, exchange, ejection and adaptive DFS operate through the common benchmark evaluation path. The paired fleet analysis contains all 600 benchmark instances, representing 40,800 customers and 180,000 items. A complete 600-run trajectory archive supplies matched distance and search-time statistics. Source, manifest, result and coordinate records provide a reproducible chain from input instance to reported outcome.

Table 3 Experimental design

Design element	Specification	Purpose
Instance matrix	3 customer levels × 2 item levels × 3 type levels	18 controlled strata
Paired fleet outcomes	600/600	Complete benchmark denominator
Search budget	1800 s	Tiered difficult-instance evaluation
Compute unit	One CPU thread per run	Comparable resource accounting
Primary endpoint	Paired change in vehicle count	Fleet consolidation
Secondary endpoint	Paired route-distance change	Operational trade-off
Uncertainty	20,000 paired-instance bootstrap resamples	95% confidence interval
Feasibility endpoint	Benchmark validation and retained coordinates	Auditability
Service volume	40,800 customers; 180,000 items	Fleet-resource intensity denominator

Table 3 separates the complete fleet endpoint from the trajectory endpoint. Vehicle-count effects use all 600 paired outcomes, while distance and search timing use the 600 matched runs containing the complete trajectory record. Bootstrap intervals use the 600 paired vehicle-saving observations and 20,000 instance-level resamples following the resampling principle of Efron and Tibshirani [47].

5.3. Evaluation Measures

The primary effect is the paired saving $\Delta N = N_{initial} - N_{final}$. Aggregate reduction divides the sum of ΔN by the total initial fleet. Improvement frequency records the number of pairs with ΔN>0, while the conditional saving describes magnitude among improved instances. Search dynamics use the first and last certified fleet-reduction times. Route-distance analysis retains ΔD to distinguish joint improvements from consolidation trade-offs.

6. Results

6.1. Primary Fleet-Consolidation Effect

H-ALNS produces a large and directionally consistent fleet effect across the complete benchmark. The aggregate fleet decreases from 9346 to 7915 vehicles. The resulting 1431 avoided dispatches correspond to a 15.31% aggregate reduction. Vehicle demand decreases in 340 instances and remains equal in 260 instances; no paired outcome returns to a larger fleet. The mean paired saving is 2.385 vehicles, with a 95%

paired-instance bootstrap interval of 2.128–2.648 vehicles. Relative to fixed service volume, fleet intensity decreases from 22.91 to 19.40 vehicles per 100 customers and from 51.92 to 43.97 vehicles per 1000 items.

Table 4 Paired fleet-consolidation outcomes

Endpoint	Estimate	Uncertainty or denominator	Decision meaning
Paired fleet outcomes	600	600/600 benchmark instances	Complete primary evidence set
Aggregate fleet	9346 → 7915	1431 vehicles avoided	15.31% reduction
Paired outcome	340 / 260 / 0	Improved / equal / increased	56.67% cross a fleet threshold
Mean paired saving	2.385 vehicles	95% bootstrap CI 2.128–2.648	Average resource effect
Saving when improved	4.21 vehicles	Median 3; maximum 14	Magnitude after threshold crossing
Relative saving per instance	Mean 10.26%	Median 7.69%; maximum 70.59%	Instance-normalized effect
Time to first reduction	50.95 s	Median in 600-run trajectory archive	Early search productivity
Time to final reduction	702.20 s	Median in 600-run trajectory archive	Continued improvement
Fleet intensity / 100 customers	22.91 → 19.40	40,800 customers	15.31% lower
Fleet intensity / 1000 items	51.92 → 43.97	180,000 items	15.31% lower

Table 4 separates effect frequency, effect magnitude and service-volume intensity. The 56.67% improvement frequency shows how often H-ALNS closes at least one vehicle, whereas the conditional mean of 4.21 vehicles shows the consolidation achieved once the threshold is crossed. Both normalized intensities decrease by the same 15.31% aggregate rate because the customer and item demand is fixed across the paired comparison.

Fig. 3 visualizes the result from four complementary perspectives. Panels (a)–(c) use all 600 paired fleet outcomes to compare customer scales, instance size, box-type heterogeneity and the full saving distribution. Panel (d) uses the 600-run trajectory archive to report the median time to the first and final reduction. The panels therefore connect effect magnitude, coverage and search timing.

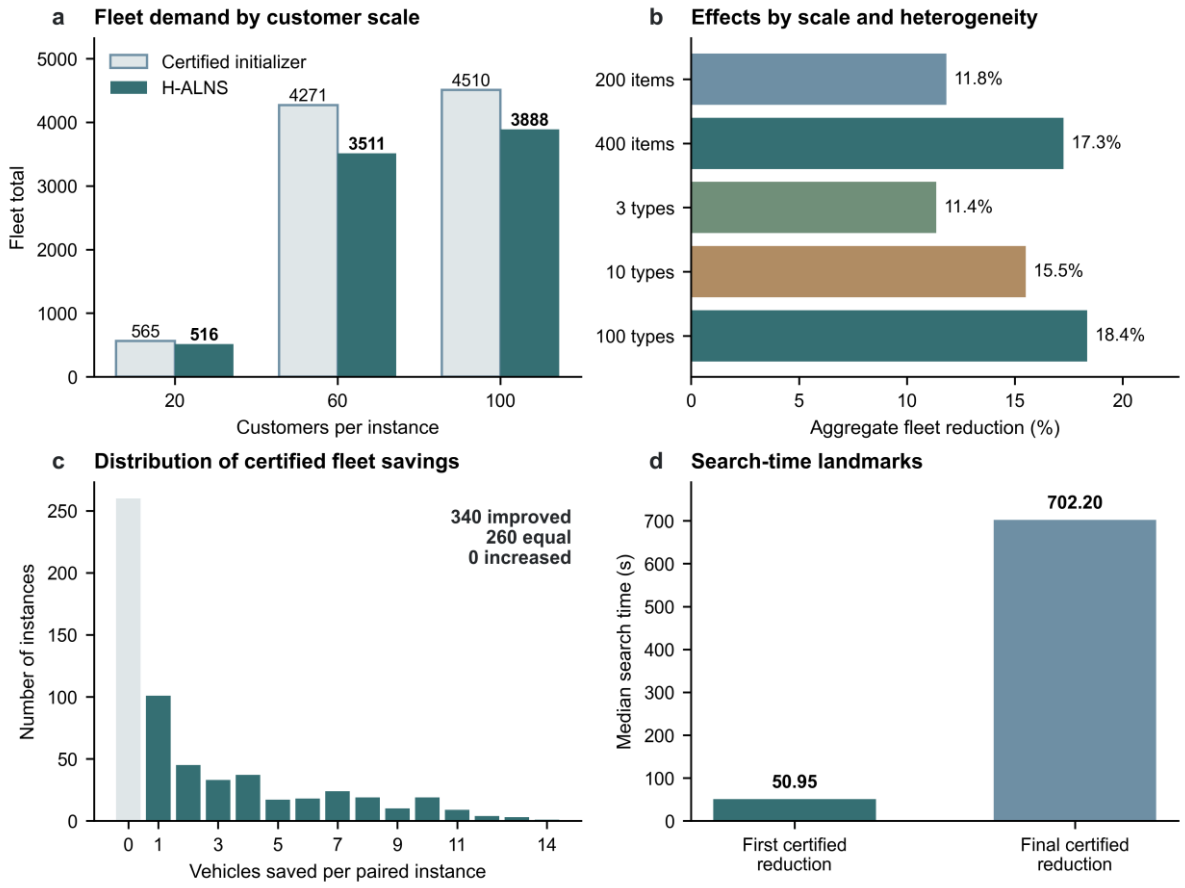


Fig. 3 Certified fleet-resource effects across 600 paired instances; panels a–c use the full benchmark and panel d uses 600 complete trajectory records

6.2. Effect Consistency across Benchmark Factors

The aggregate reduction is positive at every customer, item and box-type level. The effect is 8.67% for 20 customers, rises to 17.79% for 60 customers and remains 13.79% for 100 customers. Increasing geometric scale strengthens the result: the reduction is 11.83% for 200 items and 17.26% for 400 items. Box-type heterogeneity produces the same progression, from 11.36% at three types to 18.36% at 100 types.

Table 5 Factor-stratified fleet effects

Factor	Level	Paired instances	Improved, n (%)	Aggregate fleet, N0 → N*	Saved	Reduction (%)	Mean saved
Customers	20	120	36 (30.0%)	565 → 516	49	8.67%	0.41
Customers	60	240	159 (66.2%)	4271 → 3511	760	17.79%	3.17
Customers	100	240	145 (60.4%)	4510 → 3888	622	13.79%	2.59
Items	200	300	155 (51.7%)	3357 → 2960	397	11.83%	1.32
Items	400	300	185 (61.7%)	5989 → 4955	1034	17.26%	3.45
Box types	3	200	106 (53.0%)	2790 → 2473	317	11.36%	1.58
Box types	10	200	117 (58.5%)	3141 → 2654	487	15.50%	2.44

Factor	Level	Paired in-stances	Improved, n (%)	Aggregate fleet, N0 → N*	Saved	Reduction (%)	Mean saved
Box types	100	200	117 (58.5%)	3415 → 2788	627	18.36%	3.13

Table 5 separates improvement frequency from aggregate reduction because the two measures answer different questions. The frequency records how often a factor level contains a successful closure, whereas the reduction incorporates the number of vehicles removed in each successful case. The 400-item and 100-type groups combine high improvement frequency with the largest aggregate reductions, supporting the structural role of exchange and ejection under more heterogeneous packing conditions.

Fig. 4 resolves the aggregate result into the complete factorial benchmark structure. The two panels separate the 200-item and 400-item groups, while rows identify customer count and columns identify box-type count. Each cell reports both the percentage fleet reduction and the number of paired instances, allowing effect size and evidence coverage to be read together before the complete numerical values are listed in Table 6.

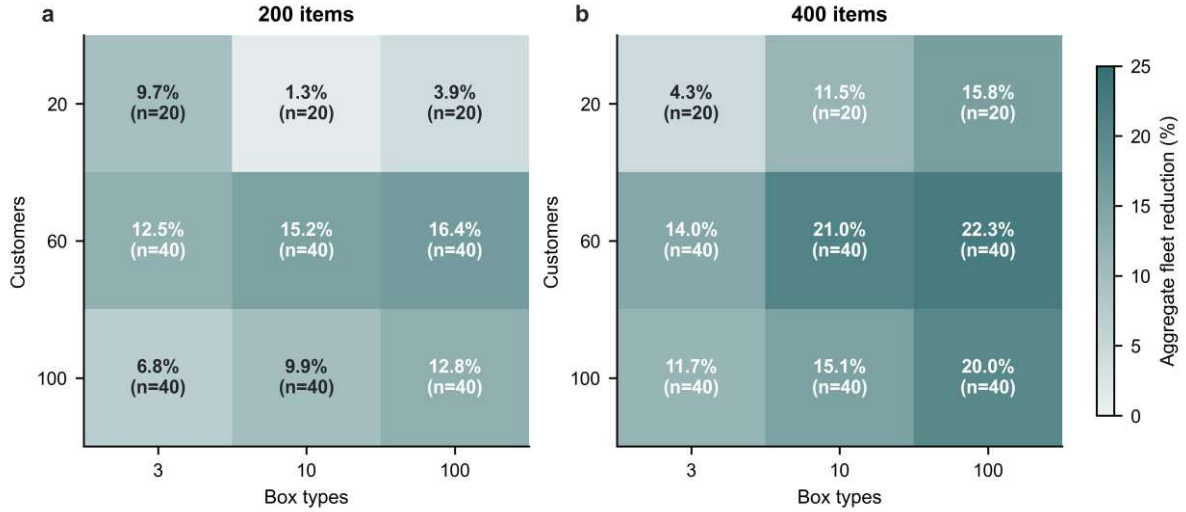


Fig. 4 Aggregate fleet reduction across all 18 customer–item–box-type strata

6.3. Complete 18-Stratum Pattern

Table 6 reports every factorial stratum. In the first column, C/I/BT denotes customers, items and box types. N0 and N* denote the aggregate certified fleet before and after H-ALNS, respectively; all percentages use N0 as the denominator.

Table 6 Benchmark-stratum fleet consolidation

Stratum (C/I/BT)	Paired in-stances	Improved, n (%)	Aggregate fleet, N0 → N*	Vehicles saved	Fleet reduction (%)
20/200/3	20	7 (35.0%)	72 → 65	7	9.72%
20/200/10	20	1 (5.0%)	77 → 76	1	1.30%
20/200/100	20	3 (15.0%)	76 → 73	3	3.95%
20/400/3	20	3 (15.0%)	94 → 90	4	4.26%

Stratum (C/I/BT)	Paired instances	Improved, n (%)	Aggregate fleet, N0 → N*	Vehicles saved	Fleet reduction (%)
20/400/10	20	9 (45.0%)	113 → 100	13	11.50%
20/400/100	20	13 (65.0%)	133 → 112	21	15.79%
60/200/3	40	24 (60.0%)	471 → 412	59	12.53%
60/200/10	40	26 (65.0%)	508 → 431	77	15.16%
60/200/100	40	27 (67.5%)	538 → 450	88	16.36%
60/400/3	40	25 (62.5%)	800 → 688	112	14.00%
60/400/10	40	32 (80.0%)	927 → 732	195	21.04%
60/400/100	40	25 (62.5%)	1027 → 798	229	22.30%
100/200/3	40	20 (50.0%)	482 → 449	33	6.85%
100/200/10	40	25 (62.5%)	545 → 491	54	9.91%
100/200/100	40	22 (55.0%)	588 → 513	75	12.76%
100/400/3	40	27 (67.5%)	871 → 769	102	11.71%
100/400/10	40	24 (60.0%)	971 → 824	147	15.14%
100/400/100	40	27 (67.5%)	1053 → 842	211	20.04%

Table 6 confirms a positive aggregate fleet reduction in all 18 strata. The strongest stratum is 60 customers, 400 items and 100 box types, where 25 of 40 pairs improve and the aggregate fleet decreases by 22.30%. The 60-customer, 400-item, 10-type stratum reaches 21.04%, while the 100-customer, 400-item, 100-type stratum reaches 20.04%. This consistency shows that the aggregate result is distributed across the factorial design rather than concentrated in one instance family.

6.4. Fleet–Distance Outcomes

Within the 600-run trajectory archive, the fleet-distance pairs distinguish joint improvements from consolidation trade-offs. Twenty solutions reduce both vehicle count and route distance. A further 314 solutions use fewer vehicles with a longer route, while 266 remain on the initial fleet and distance layer. This classification shows whether fleet closure reinforces or trades against route efficiency.

Table 7 Fleet–distance outcome classes

Outcome class	Cases	Fleet effect	Distance effect	Operational interpretation
Joint resource improvement	20	$\Delta N > 0$	$\Delta D < 0$	Fewer vehicles and shorter routes
Fleet consolidation trade-off	314	$\Delta N > 0$	$\Delta D > 0$	Fewer vehicles with longer routes
Stable trajectory layer	266	$\Delta N = 0$	$\Delta D = 0$	Initializer fleet and distance retained

Table 7 separates the two forms of operational gain. Joint improvements strengthen fleet and route efficiency simultaneously, whereas consolidation trade-offs quantify the additional travel associated with closing vehicles. The paired classification therefore complements the aggregate fleet-reduction result.

6.5. Best Instance-Level Fleet Results

Table 8 Largest paired fleet reductions

Instance	C/I/BT	Initial N	Final N	Saved	Reduction (%)
434_n060_m400_bt100	60/400/100	43	29	14	32.56%
546_n100_m400_bt10	100/400/10	55	42	13	23.64%
368_n060_m400_bt10	60/400/10	44	31	13	29.55%
567_n100_m400_bt100	100/400/100	19	6	13	68.42%
482_n100_m400_bt3	100/400/3	55	43	12	21.82%
523_n100_m400_bt100	100/400/100	47	35	12	25.53%
493_n100_m400_bt100	100/400/100	46	34	12	26.09%
600_n100_m400_bt100	100/400/100	17	5	12	70.59%
462_n060_m400_bt100	60/400/100	45	34	11	24.44%
491_n100_m400_bt100	100/400/100	45	34	11	24.44%

Table 8 shows that the largest fleet transitions recur across several customer and heterogeneity settings. Instance 434_n060_m400_bt100 removes 14 of 43 vehicles. Three instances remove 13 vehicles, including the 60-customer 400-item case 368, the 100-customer 400-item case 546 and instance 567 after coordinate-level reconstruction. The top-ranked set therefore combines large absolute savings with broad factorial coverage.

7. Discussion

7.1 Intelligence arises from certified decision feedback

The full-benchmark evidence attributes fleet consolidation to an intelligence loop rather than to an algorithm label alone. Geographic reassignment proposes service-compatible receiver routes; exchange and ejection alter saturated customer combinations; adaptive DFS resolves the remaining geometric barrier. Each proposal is judged through complete coordinate reconstruction, and its certified gain or classified failure updates subsequent operator priorities. The observed 1431-vehicle reduction therefore emerges from repeated interaction between route structure, packing evidence and feedback.

7.2 Resource efficiency across scale and heterogeneity

Resource gains persist across every customer, item and box-type level. The stronger reductions in 400-item and high-heterogeneity strata show that structural neighborhoods become more valuable as direct greedy insertion loses expressive power. At the service-volume level, fleet intensity falls by 15.31%, from 22.91 to 19.40 vehicles per 100 customers and from 51.92 to 43.97 vehicles per 1000 items. These normalized measures connect the optimization result to the resource-efficiency logic represented by SDGs 8 and 12 [4].

7.3 Fleet thresholds and route-distance consequences

Fleet efficiency changes when customer regrouping crosses an integer vehicle-demand threshold. The 340 improved instances show how often that threshold is

reached, while the conditional saving of 4.21 vehicles describes its magnitude. Route distance then identifies the operational consequence of consolidation: 20 trajectory pairs improve both fleet size and distance, while the other fleet reductions quantify the travel associated with a more consolidated service structure. This two-level interpretation preserves the primacy of fleet resources and keeps route quality visible.

7.4 Integration with Industry 4.0 freight systems

H-ALNS fits a digital freight architecture in which order records, item master data, vehicle capacity, travel information and time windows enter a shared optimization service. The service returns customer routes, loading coordinates, a feasibility certificate and fleet-resource indicators. A transport management system can use the routes and fleet layer for dispatch planning, while a warehouse execution system can use the coordinates for loading guidance. The same decision object therefore links planning, physical execution and sustainability measurement in an intelligence-driven logistics workflow.

8. Conclusions

This study presents an intelligence-driven approach to customer-indivisible three-dimensional route loading. H-ALNS combines dual certified initialization, geographic reassignment, whole-vehicle closure, two-route exchange, three-route ejection, failure-feedback operator learning and adaptive depth-first packing. A shared decoder and validator maintain direct correspondence between customer-level search decisions and complete item coordinates.

Across 600 benchmark instances and 18 factorial strata, the method reduces the aggregate fleet from 9346 to 7915 vehicles. The 1431 avoided dispatches represent a 15.31% reduction; 340 instances improve, 260 remain equal and none increase. Fleet intensity consequently falls from 22.91 to 19.40 vehicles per 100 customers and from 51.92 to 43.97 vehicles per 1000 items. Positive aggregate reductions in every stratum demonstrate that the resource effect extends across service scale, geometric scale and box-type heterogeneity.

The study establishes a measurable sustainability mechanism for intelligent freight operations: route-level learning proposes customer consolidation, coordinate-level reconstruction proves physical executability, and certification converts the result into auditable fleet-resource evidence. This closed decision loop supplies a practical optimization component for resource-efficient freight planning and digitally coordinated logistics.

Author contributions: Junling Zhu contributed to conceptualization, methodology, software, formal analysis, data curation, visualization, and writing the original draft. Tang-Xi Chen contributed to methodology, validation, formal analysis, and reviewing and editing the manuscript. Yujie Lin contributed to conceptualization, resources, supervision, project administration, funding acquisition, and reviewing and editing the manuscript. Shiyi Tan contributed to investigation, validation, data curation, visualization, and reviewing and editing the manuscript. Mingjun Qiu contributed to validation and reviewing and editing the manuscript. All authors reviewed and approved the final manuscript.

Funding: This research was supported by the Zhaoqing University Grant (QN202449); the project 'Decision Support for Public Opinion Governance Based on Artificial Intelligence and Big Data'; and the ESI Discipline Enhancement Program of Zhaoqing University.

Data availability: The benchmark instances analysed in this study were created by Krebs, Ehmke and Koch and are publicly available at[https://github.com/CorinnaKrebs/Instances/tree/master/Krebs_Ehmke_Koch_2021]. The computational data generated in this study, including per-instance run records, loading-solution certificates and the data underlying the reported tables and figures, are available from the corresponding author upon reasonable request.

Clinical trial number: not applicable.

Ethics, Consent to Participate, and Consent to Publish declarations: not applicable.

References

1. Barreto, L.; Amaral, A.; Pereira, T. Industry 4.0 implications in logistics: An overview. Procedia Manuf. 2017, 13, 1245-1252. https://doi.org/10.1016/j.promfg.2017.09.045.
2. Yavas, V.; Ozkan-Ozen, Y.D. Logistics centers in the new industrial era: A proposed framework for Logistics Center 4.0. Transp. Res. Part E Logist. Transp. Rev. 2020, 135, 101864. https://doi.org/10.1016/j.tre.2020.101864.
3. Winkelhaus, S.; Grosse, E.H. Logistics 4.0: A systematic review towards a new logistics system. Int. J. Prod. Res. 2020, 58, 18-43. https://doi.org/10.1080/00207543.2019.1612964.
4. United Nations. Goal 8: Promote sustained, inclusive and sustainable economic growth, full and productive employment and decent work for all. United Nations Department of Economic and Social Affairs. https://sdgs.un.org/goals/goal8. Accessed 30 September 2026.
5. United Nations. Goal 12: Ensure sustainable consumption and production patterns. United Nations Department of Economic and Social Affairs. https://sdgs.un.org/goals/goal12. Accessed 30 September 2026.
6. George, J.A.; Robinson, D.F. A heuristic for packing boxes into a container. Comput. Oper. Res. 1980, 7, 147-156. https://doi.org/10.1016/0305-0548(80)90001-5.
7. Bischoff, E.E.; Ratcliff, M.S.W. Issues in the development of approaches to container loading. Omega 1995, 23, 377-390. https://doi.org/10.1016/0305-0483(95)00015-G.
8. Crainic, T.G.; Perboli, G.; Tadei, R. Extreme point-based heuristics for three-dimensional bin packing. INFORMS J. Comput. 2008, 20, 368-384. https://doi.org/10.1287/ijoc.1070.0250.
9. Gehring, H.; Bortfeldt, A. A genetic algorithm for solving the container loading problem. Int. Trans. Oper. Res. 1997, 4, 401-418. https://doi.org/10.1111/j.1475-3995.1997.tb00095.x.
10. Gonçalves, J.F.; Resende, M.G.C. A biased random-key genetic algorithm for 2D and 3D bin packing problems. Int. J. Prod. Econ. 2013, 145, 500-510. https://doi.org/10.1016/j.ijpe.2013.04.019.
11. Junqueira, L.; Morabito, R.; Yamashita, D.S. Three-dimensional container loading models with cargo stability and load bearing constraints. Comput. Oper. Res. 2012, 39, 74-85. https://doi.org/10.1016/j.cor.2010.07.017.
12. Davies, A.P.; Bischoff, E.E. Weight distribution considerations in container loading. Eur. J. Oper. Res. 1999, 114, 509-527. https://doi.org/10.1016/S0377-2217(98)00139-8.
13. Krebs, C.; Ehmke, J.F. Axle weights in combined vehicle routing and container loading problems. EURO J. Transp. Logist. 2021, 10, 100043. https://doi.org/10.1016/j.ejtl.2021.100043.
14. Pollaris, H.; Braekers, K.; Caris, A.; Janssens, G.K.; Limbourg, S. Vehicle routing problems with loading constraints: State-of-the-art and future directions. OR Spectrum 2015, 37, 297-330. https://doi.org/10.1007/s00291-014-0386-3.
15. Pisinger, D. Heuristics for the container loading problem. Eur. J. Oper. Res. 2002, 141, 382-392. https://doi.org/10.1016/S0377-2217(02)00132-7.
16. Eley, M. Solving container loading problems by block arrangement. Eur. J. Oper. Res. 2002, 141, 393-409. https://doi.org/10.1016/S0377-2217(02)00133-9.
17. Fanslau, T.; Bortfeldt, A. A tree search algorithm for solving the container loading problem. INFORMS J. Comput. 2010, 22, 222-235. https://doi.org/10.1287/ijoc.1090.0338.

18. Bortfeldt, A.; Gehring, H. A hybrid genetic algorithm for the container loading problem. Eur. J. Oper. Res. 2001, 131, 143-161. https://doi.org/10.1016/S0377-2217(00)00055-2.
19. Araya, I.; Riff, M.C. A beam search approach to the container loading problem. Comput. Oper. Res. 2014, 43, 100-107. https://doi.org/10.1016/j.cor.2013.09.003.
20. Paquay, C.; Limbourg, S.; Schyns, M. A tailored two-phase constructive heuristic for the three-dimensional multiple bin size bin packing problem with transportation constraints. Eur. J. Oper. Res. 2018, 267, 52-64. https://doi.org/10.1016/j.ejor.2017.11.010.
21. Ma, Y.; Zhou, Y.; Fang, Q.; Xia, S.; Chen, W. A three-dimensional container loading algorithm for solving logistics packing problem. EURO J. Transp. Logist. 2025, 14, 100167. https://doi.org/10.1016/j.ejtl.2025.100167.
22. Bortfeldt, A.; Wäscher, G. Constraints in container loading-A state-of-the-art review. Eur. J. Oper. Res. 2013, 229, 1-20. https://doi.org/10.1016/j.ejor.2012.12.006.
23. Gzara, F.; Elhedhli, S.; Yildiz, B. The pallet loading problem: Three-dimensional bin packing with practical constraints. Eur. J. Oper. Res. 2020, 287, 1062-1074. https://doi.org/10.1016/j.ejor.2020.04.053.
24. do Nascimento, O.X.; Queiroz, T.A.; Junqueira, L. Practical constraints in the container loading problem: Comprehensive formulations and exact algorithm. Comput. Oper. Res. 2021, 128, 105186. https://doi.org/10.1016/j.cor.2020.105186.
25. Erbayrak, S.; Ozkir, V.; Yildirim, U.M. Multi-objective 3D bin packing problem with load balance and product family concerns. Comput. Ind. Eng. 2021, 159, 107518. https://doi.org/10.1016/j.cie.2021.107518.
26. Krebs, C.; Ehmke, J.F.; Koch, H. Advanced loading constraints for 3D vehicle routing problems. OR Spectrum 2021, 43, 835-875. https://doi.org/10.1007/s00291-021-00645-w.
27. Gendreau, M.; Iori, M.; Laporte, G.; Martello, S. A tabu search algorithm for a routing and container loading problem. Transp. Sci. 2006, 40, 342-350. https://doi.org/10.1287/trsc.1050.0145.
28. Iori, M.; Salazar-González, J.J.; Vigo, D. An exact approach for the vehicle routing problem with two-dimensional loading constraints. Transp. Sci. 2007, 41, 253-264. https://doi.org/10.1287/trsc.1060.0165.
29. Fuellerer, G.; Doerner, K.F.; Hartl, R.F.; Iori, M. Ant colony optimization for the two-dimensional loading vehicle routing problem. Comput. Oper. Res. 2009, 36, 655-673. https://doi.org/10.1016/j.cor.2007.10.021.
30. Ceschia, S.; Schaerf, A.; Stützle, T. Local search techniques for a routing-packing problem. Comput. Ind. Eng. 2013, 66, 1138-1149. https://doi.org/10.1016/j.cie.2013.07.025.
31. Krebs, C.; Fuellerer, G.; Schwindt, C. Solution validator and visualizer for combined vehicle routing and container loading problems. Ann. Oper. Res. 2023. https://doi.org/10.1007/s10479-023-05238-0.
32. Ropke, S.; Pisinger, D. An adaptive large neighborhood search heuristic for the pickup and delivery problem with time windows. Transp. Sci. 2006, 40, 455-472. https://doi.org/10.1287/trsc.1050.0135.
33. Pisinger, D.; Ropke, S. A general heuristic for vehicle routing problems. Comput. Oper. Res. 2007, 34, 2403-2435. https://doi.org/10.1016/j.cor.2005.09.012.
34. Krebs, C.; Ehmke, J.F.; Koch, H. Effective loading in combined vehicle routing and container loading problems. Comput. Oper. Res. 2023, 149, 105988. https://doi.org/10.1016/j.cor.2022.105988.
35. Küçük, M.; Yildiz, S.T. Constraint programming-based solution approaches for three-dimensional loading capacitated vehicle routing problems. Comput. Ind. Eng. 2022, 171, 108505. https://doi.org/10.1016/j.cie.2022.108505.
36. Cen, X.; Zhou, G.; Ji, B.; Yu, S.S.; Zhang, Z.; Fang, X. Modelling and heuristically solving three-dimensional loading constrained vehicle routing problem with cross-docking. Adv. Eng. Inform. 2023, 57, 102029. https://doi.org/10.1016/j.aei.2023.102029.
37. Chi, J.; He, S. Pickup capacitated vehicle routing problem with three-dimensional loading constraints: Model and algorithms. Transp. Res. Part E Logist. Transp. Rev. 2023, 176, 103208. https://doi.org/10.1016/j.tre.2023.103208.
38. Chi, J.; He, S.; Song, R. Solving capacitated vehicle routing problem with three-dimensional loading and relocation constraints. Comput. Oper. Res. 2025, 173, 106864. https://doi.org/10.1016/j.cor.2024.106864.

39. Zhang, H.; Li, Q.; Yao, X. Knowledge-guided optimization for complex vehicle routing with 3D loading constraints. In Parallel Problem Solving from Nature—PPSN XVIII; Springer: Cham, Switzerland, 2024; Volume 15148, pp. 133–148. https://doi.org/10.1007/978-3-031-70055-2_9.
40. Voigt, S.; Frank, M.; Fontaine, P.; Kuhn, H. Hybrid adaptive large neighborhood search for vehicle routing problems with depot location decisions. Comput. Oper. Res. 2022, 146, 105856. https://doi.org/10.1016/j.cor.2022.105856.
41. Friedrich, C.; Elbert, R. Adaptive large neighborhood search for vehicle routing problems with transshipment facilities arising in city logistics. Comput. Oper. Res. 2022, 137, 105491. https://doi.org/10.1016/j.cor.2021.105491.
42. Bonet Filella, G.; Trivella, A.; Corman, F. Modeling soft unloading constraints in the multi-drop container loading problem. Eur. J. Oper. Res. 2023, 308, 336–352. https://doi.org/10.1016/j.ejor.2022.10.033.
43. Nascimento, D.N.; Toledo, F.M.B.; Coelho, L.C. Logic-based Benders decomposition for the three-dimensional loading capacitated vehicle routing problem with time windows. Eur. J. Oper. Res. 2026, in press. https://doi.org/10.1016/j.ejor.2026.05.051.
44. Yıldız, G.B.; Yalçın, K.; Taşkın, H.B.; Gürek, M. Mathematical modeling and heuristic solutions for container loading and routing problem: A case study in a cable manufacturing company. Comput. Oper. Res. 2025, 182, 107115. https://doi.org/10.1016/j.cor.2025.107115.
45. Rajaei, M.; Moslehi, G.; Reisi-Nafchi, M. The split heterogeneous vehicle routing problem with three-dimensional loading constraints on a large scale. Eur. J. Oper. Res. 2022, 299, 706–721. https://doi.org/10.1016/j.ejor.2021.08.025.
46. Ruan, Q.; Zhang, Z.; Miao, L.; Shen, H. A hybrid approach for the vehicle routing problem with three-dimensional loading constraints. Comput. Oper. Res. 2013, 40, 1579–1589. https://doi.org/10.1016/j.cor.2011.11.002.
47. Efron, B.; Tibshirani, R.J. An Introduction to the Bootstrap; Chapman & Hall/CRC: Boca Raton, FL, USA, 1993. https://doi.org/10.1201/9780429246593.
48. Krebs, C.; Ehmke, J.F.; Koch, H. Instances for Combined 3D Loading and Vehicle Routing Problems; Otto-von-Guericke University Magdeburg: Magdeburg, Germany, 2020.